Received: 12 August 2019 | Revised: 8 January 2020 | Accepted: 31 January 2020

DOI: 10.1002/elsc.201900132

Engineering in Life Sciences

RESEARCH ARTICLE

Synergistically applying 1-D modeling and CFD for designing industrial scale bubble column syngas bioreactors

Flora Siebler[1] | **Alexey Lapin**[2] | **Ralf Takors**[1]

[1]Institute of Biochemical Engineering, University of Stuttgart, Stuttgart, Germany

[2]Stuttgart Research Centre Systems Biology, University of Stuttgart, Stuttgart, Germany

Correspondence
Professor Ralf Takors, Institute of Biochemical Engineering, University of Stuttgart, Allmandring 31, 70569 Stuttgart, Germany.
Email: takors@uni-stuttgart.de

Funding information
Bundesministerium für Bildung und Forschung, Grant/Award Number: FKZ031A468B

The reduction of greenhouse gas emissions and future perspectives of circular economy ask for new solutions to produce commodities and fine chemicals. Large-scale bubble columns operated by gaseous substrates such as CO, CO_2, and H_2 to feed acetogens for product formations could be promising approaches. Valid in silico predictions of large-scale performance are needed to dimension bioreactors properly taking into account biological constraints, too. This contribution deals with the trade-off between sophisticated spatiotemporally resolved large-scale simulations using computationally intensive Euler–Euler and Euler–Lagrange approaches and coarse-grained 1-D models enabling fast performance evaluations. It is shown that proper consideration of gas hold-up is key to predict biological performance. Intrinsic bias of 1-D models can be compensated by reconsideration of Sauter diameters derived from uniquely performed Euler–Lagrange computational fluid dynamics.

KEYWORDS

1-D model approach, bubble column reactor, computational fluid dynamics, pseudo-stationary gas gradient, two-phase Euler–Euler simulation

1 | INTRODUCTION

The Paris Climate Agreement that entered into force in November 2016 created the framework for national contributions to limit the global temperature rise well below 2°C. As such, the reduction of greenhouse gas emissions became part of responsible chemical industry leadership, now aiming to establish a circular economy [1], that is, preventing any carbon losses and ensuring economic and ecological sustainability [2, 3].

Accordingly, using CO_2, H_2, and CO gas mixtures either from gasification of municipal waste, biogenic sources or as off-gas (e.g., from steel industry) is an attractive source of reduced carbon (CO) and H_2. The so-called syngas fermentations with acetogens such as *Clostridiae* sp. are highly promising to access not only natural products (ethanol, acetate, or 2,3-butanediol) [4, 5] but also recombinant compounds such as acetone and butanol [6–8]. Those commodities require for simple, continuously operating large-scale bioreactors that could be designed as bubble columns.

Dimensioning needs thorough in silico parameter analysis to ensure proper, large-scale production. However, large-scale bubble columns are very challenging to simulate, actually comprising three phases (liquid, bubbles, and cells), turbulent flows, mass transfer of poorly soluble gases (CO, H_2), microbial reaction kinetics, and—last but not least—proper bubble population models for predicting mass transfer areas. With the advent of gaseous substrates for large-scale single cell protein production in the 1970 s, the attraction of bubble columns peaked but somewhat leveled out during the last

Abbreviation: CFD, computational fluid dynamics.

decades. Intensive studies in 6–10 m pilot scales [10, 13] unraveled correlations between gas velocities and k_La and even succeeded to develop 1-D models for predicting gas transfers properly [11]. The applicability of the well-known k-ε model for bubble columns was questioned [12, 14] outlining the need to consider turbulent flow regimes properly. Nevertheless, 1-D modeling of bubble columns should be possible, in particular when iterative optimization cycles are taken into account [9, 13].

Ideally, large-scale simulations should consider spatiotemporal heterogeneities and their impact on cellular performance [9–12]. But related simulations not only require thorough mechanistic models but also sufficient computational power [13]. Accordingly, simplifications are often made either by assuming ideal mixing, 1-D gas gradients [14] or dissembling the large bioreactor into numerous volumes [15–19].

Recent highly valuable examples are given by Chen et al. [20, 21] who evaluated the performance of large-scale *Clostridiae* fermentations with the help of a genome-scale metabolic model applying spatiotemporal bioreactor simulations based on homogenously mixed volumes. The authors applied flux balance analysis to estimate flux distributions for each 1-D discretization. However, despite successful application, growth rates were overestimated by trend and physical criteria such as gas hold-up were not integrated, yet. The latter may have affected the large-scale prediction accuracy, too.

Without doubt, such 1-D models require less computational efforts than sophisticated Euler–Lagrange computational fluid dynamics (CFD). They offer relatively easy-to-implement use but may hide intrinsic drawbacks hampering prediction quality. Furthermore, their predictions might be biased because model granularity is intrinsically coarse. Nevertheless, they are the method of choice in conceptual design to search in operational parameter spaces. This contribution exactly deals with the trade-off between properly simulating large-scale bubble column performance and screening operational parameter spaces with reasonable computational effort. Special emphasis will be put on the impact of gas hold-up on the expected biological performance, that is, product-per-biomass yield. This relation is considered of particular importance as it links a key operational parameter with the most important biological readout.

PRACTICAL APPLICATION

Transferring biochemical processes from the laboratory to industrial scales is very challenging. Physical properties may change drastically and may cause nonwanted performance losses. Accordingly, tools are needed to predict large-scale conditions leading to an optimum design with minimized performance losses.

This study presents a computational tool for conceptual reactor design of an industrial-scale bubble column bioreactor. Time-consuming and computationally challenging design parameter studies were performed with a simplified 1-D model. Noteworthy, key settings including gas hold-up were derived from spatially resolved, computational fluid dynamics (CFD). The interaction of both approaches represents the optimum trade-off between computationally intensive CFD and the essential probing of a broad design parameter space performed via 1-D modeling.

2 | MATERIALS AND METHODS

2.1 | Geometry, reactor set-up, and biological system

Both simulation approaches were conducted for equal reactor geometry using the same biological system, that is, *Clostridium ljungdahlii* DSM 13528 that grows on carbon monoxide as C-source. The choice of CO simplifies the comparison with the previous publication [11] and represents the preferred carbon and electron source for alcohol production. A cylindrical reactor with 25 m liquid height and diameter $D_R = 2.52$ m was chosen resulting in a H_L/D_R-ratio of about 10. Consequently, the setup imposed high hydrostatic pressure gradients. For 1-D modeling, the bubble column simulations considered continuous countercurrent mode with liquid recycling and medium feed at the top of the reactor. At the bottom, synthesis gas was continuously provided via the total cross-sectional area A_R. The media density ρ_L was assumed to be similar to the properties of water with $\rho_L = 1{,}000$ kg m^{-3}. Isothermal process conditions were assumed with an operating temperature of 310.15 K. Heat generation was neglected. Nevertheless, in large-scale bioreactors temperature control might be necessary. No additional pressure was applied beside the ambient pressure of 1 atm and the hydrostatic pressure due to the column height.

State variables such as gas concentrations and gas hold-up were partially differentiated following the scheme presented by Chen et al. [14].

2.1.1 | 1-D approach

This approach is similar to the publications of Chen et al. [14, 20, 21]. The new mass balance equations are described in this section. Growth and production formation are calculated as described in Siebler et al. [11]. Spatial and temporal discretization was kept the same as in Chen et al. [14, 21] and is described in more detail in the Supporting Information. According to the reactor set-up outlined in the previous section, four partial differential equations and four ordinary

differential equations need to be set. Dissolved and gaseous synthesis gas components, the gas hold-ups, and the bubble number density are local, time dependent variables, and serve as input values for calculating dynamics of growth and product formation.

The mass balance for the liquid phase of one discretization volume is derived including convective and diffusive transport, phase-to-phase mass transfer, and consumption terms. The volume of each section is written as: $\Delta V_L = \Delta z A_L$, where Δz is the section height and A_L is the liquid surface area between the sections. The cross-sectional area of the reactor A_R is the sum of A_L and the gaseous interface A_G. The gaseous and liquid volume fractions are indicated by ε_G and ε_L (see Figure S2). It follows

$$\begin{aligned}\frac{\Delta z\, \mathrm{d}c_L A_L}{\mathrm{d}t} = &\underbrace{A_L c_L v_{L,\mathrm{slip}}\Big|_{z+\Delta z} - A_L c_L v_{L,\mathrm{slip}}\Big|_{z}}_{\text{transport}} \\ &+ \underbrace{A_{\mathrm{bubbles}} k_L \left(c_L^* - c_L\right)}_{\text{mass transfer}} \underbrace{- \Delta z A_L q_c c_X}_{\text{consumption}} \\ &+ \underbrace{D_L A_L \frac{\mathrm{d}c_L}{\mathrm{d}z}\Big|_{z+\Delta z} - D_L A_L \frac{\mathrm{d}c_L}{\mathrm{d}z}\Big|_{z}}_{\text{diffusion}} \end{aligned} \quad (1)$$

with A_{bubbles} as the mass transfer area between the liquid and gaseous phase that leads to $a = A_{\mathrm{bubbles}}/(\Delta z A_L)$ and the well-known $k_L a$ term for modeling the mass transfer term with the equilibrium concentration c_L^* and the soluble gas concentration c_L. The liquid slip velocity $v_{L,slip}$ multiplied by $\varepsilon_L = 1 - \varepsilon_G$ gives the liquid velocity v_L, which can be assumed to be constant. The diffusion term with the liquid phase dispersion coefficient D_L with 4.5 $\mathrm{m^2\ h^{-1}}$ [21] is included as well as the consumption term consists of the uptake kinetic q_c and biomass concentration c_X. By dividing equation (1) by A_R and Δz and using the correlation $1 - \varepsilon_G = A_L / A_R$, the final partial differential equations for the dissolved gases ($m \in [\mathrm{CO}, \mathrm{CO_2}, \mathrm{H_2}]$) can be formulated.

$$\begin{aligned}\frac{\partial c_{L,m}\varepsilon_L}{\partial t} = &\, v_{L,\mathrm{slip}} \frac{\partial c_{L,m}\varepsilon_L}{\partial z} + k_{L,m} a \left(c_{L,m}^* - c_{L,m}\right) \\ &- q_m c_X \varepsilon_L + D_L \frac{\partial^2 c_{L,m}\varepsilon_L}{\partial z^2}\end{aligned} \quad (2)$$

Each balance of the gas phase only needs to consider convective mass transport and phase-to-phase mass transfer that leads to

$$\frac{\partial c_{G,m}\varepsilon_G}{\partial t} = v_{G,slip} \frac{\partial c_{G,m}\varepsilon_G}{\partial z} - k_{L,m} a \left(c_{L,m}^* - c_{L,m}\right) \quad (3)$$

Because the gas phase is compressible, the gas hold-ups depend on the local pressure that correlate ε_L and ε_G with the liquid height H_L. The total molar density ρ^* is introduced using the ideal gas law $PV = nRT$ and the hydrostatic pressure $P_H = P_0 + \rho g h$ with $h = H_L - z$

$$\rho^* = \sum_{m=1}^{3} \frac{\rho_m(z)}{M_m} = \frac{P_0 + \left(H_L - z\right) g \rho_L \varepsilon_L}{RT} \quad (4)$$

with the gravitational acceleration g, liquid density ρ_L, universal gas constant R, and the operating temperature T. The index $m = 1, 2, 3$ always represents the synthesis gas composition with CO, CO_2, and H_2. Considering the total molar gas density, the following equation can be derived:

$$\frac{\partial \varepsilon_G \rho^*}{\partial t} = v_{G,\mathrm{slip}} \frac{\partial \varepsilon_G \rho^*}{\partial z} - \sum_{m=1}^{3} k_{L,m} a \left(c_{L,m}^* - c_{L,m}\right) \quad (5)$$

It is further assumed that the number density n_G, that is, the number of bubbles N_B divided by the reactor volume V_R, only depends on convection. No further bubble breakage or coalescence occurs.

$$\begin{aligned}\tfrac{\partial n_G}{\partial t} &= v_{G,\mathrm{slip}} \tfrac{\partial n_G}{\partial z} \\ n_G\ (t, z) &= \tfrac{N_B}{V_R} = \tfrac{\varepsilon_G}{\frac{4}{3}\pi R_B^3}\end{aligned} \quad (6)$$

Nevertheless, the bubble radius R_B is a function of the gas hold-up and hydrostatic pressure. If the number of bubbles in a section i is multiplied with the bubble volume $V_{B,i}$, the gas hold-up $\varepsilon_{G,i}$ is derived. Therefore, all balance equations are intertwined by the gas hold-up. Noteworthy, this also affects the volumetric surface area a, which is the sum of all bubble surfaces A_B divided by the reactor volume.

$$a = \frac{\sum A_B}{V_R} = \frac{3}{R_B} \varepsilon_G \quad (7)$$

Product formation and growth are formulated as ordinary differential equations (see Equations 8) using the growth rate μ and the dilution rate $D = 0.055\ \mathrm{h^{-1}}$.

$$\begin{aligned}\frac{\mathrm{d}c_X}{\mathrm{d}t} &= \mu c_X - D c_X \\ \frac{\mathrm{d}c_k}{\mathrm{d}t} &= M_k\, q_k c_X - D c_k\end{aligned} \quad (8)$$

Because biomass and product concentrations c_k are in $\mathrm{g\ L^{-1}}$, the molecular weight M_k is needed with $k \in$ [acetate, ethanol, 2,3−butanediol]. For the sake of simplicity, individual production rates q_k represent mean values of the section-specific $q_{k,i}$ that consider local gas uptake kinetics $q_{m,i}$ (see Supporting Information).

2.2 | Computational fluid dynamics

Recently, the set-up of the simulation framework including results has been published in Siebler et al. [11]. Accordingly, only a draft explanation is given. For details, readers are

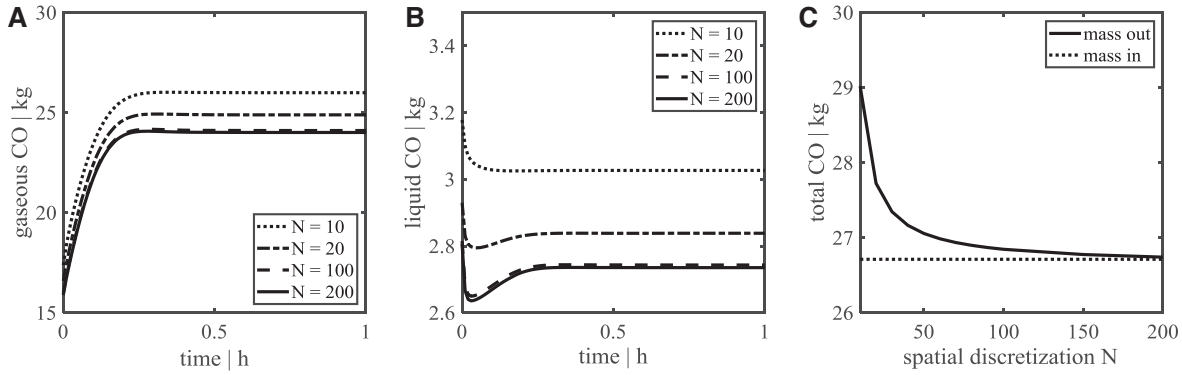

FIGURE 1 Refinement study. In (A) and (B), the gaseous and dissolved (liquid) mass of CO over times is shown. Exemplary, four discretization steps are depicted $N = 10$, 20, 100, and 200. In (C), the relation between total CO leaving and entering the column is illustrated revealing that $N = 100$ closes the mass balance with less than 5% gap

referred to the publication. Euler–Euler two phase simulations were conducted with the CFD tool ANSYS Fluent 18.0. The Reynolds-averaged Navier–Stokes equations combined with the re-normalization group k-ε-model were solved to derive pseudo-stationary gas gradients similar to the 1-D approach. Drag and lift forces, wall lubrication, turbulent dispersion, and interaction as well as breakage and coalescence were enabled. For mass transfer, the same correlation as in Equation (9) was used except for the bubble diameter d_B, which was exchanged by the Sauter mean bubble diameter d_{32}. For the solubility of the gas, the Henry law was also applied. Pressure was considered as static. The initial bubble size was 4 mm. To model CO uptake kinetics, the correlation of Mohammadi et al. [22] was used (see Supporting Information eq. 13). The analyzed fermentation "snap-shot" operation window was defined by chosen the biomass concentration of 10 g L^{-1}.

As indicated for the 1-D approach, the uptake kinetics of CO were translated into production rates according to the approximation described in Siebler et al. [11]. So far, there is no comprehensive model for the prediction of production rates of *C. ljungdahlii*. The simple correlation used does neither include internal redox and energy balances nor maintenance. It is solely based on the element balances of carbon, hydrogen, and oxygen. Nevertheless, the correlation allows to compare both modeling approaches.

3 | RESULTS

3.1 | Basic settings of 1-D

The bubble column was divided in N slices each consisting of a liquid L and a gaseous G fraction with the uprising superficial gas velocity v_S and the downcoming liquid velocity v_L. Homogenous conditions were assumed in each liquid and gaseous phase. For identifying the number N of essential volumes (sections), simulations were performed probing N between 10 and 200 (Figure 1).

Physical state variables were simulated according to Equations (1)–(8). Biochemical reaction rates reflecting microbial metabolic activity were set as described in "Materials and Methods" section and in Siebler et al. [11].

As presented in Figure 1, the mass balance for the chosen discretization does not close but gives reasonable results for $N \geq 100$. No significant improvement of simulation accuracy and convergence could be achieved increasing N from 100 to 200. With respect to computational efforts, $N = 100$ was used for all calculations.

3.2 | Probing the parameter space

For evaluating a proper parameter setting, key impact factors defining the performance of a biotechnological bubble column need to be specified. To characterize the biological output, $Y_{PX}(SS)$ and $C_{fix}(SS)$ were chosen indicating the product per biomass yield and the metabolized amount of carbon under steady-state operating conditions, respectively. The physical operation was qualified by the total mean gas hold-up $\bar{\varepsilon}_G$, the mean bubble diameter $\bar{d}_B$, the mean oxygen transfer coefficient $\overline{k_L a}$, and the bubble number density n_G.

The simulation of the said performance criteria crucially depends on the proper prediction of $k_L a$ and their interaction with the gas hold-up ε_G and the superficial gas velocity v_S. The well-known Higbie correlation [23] was used for estimating k_L as

$$k_L = \frac{2}{\sqrt{\pi}} \left(\frac{v_T D_{CO}}{d_B} \right)^{0.5} \tag{9}$$

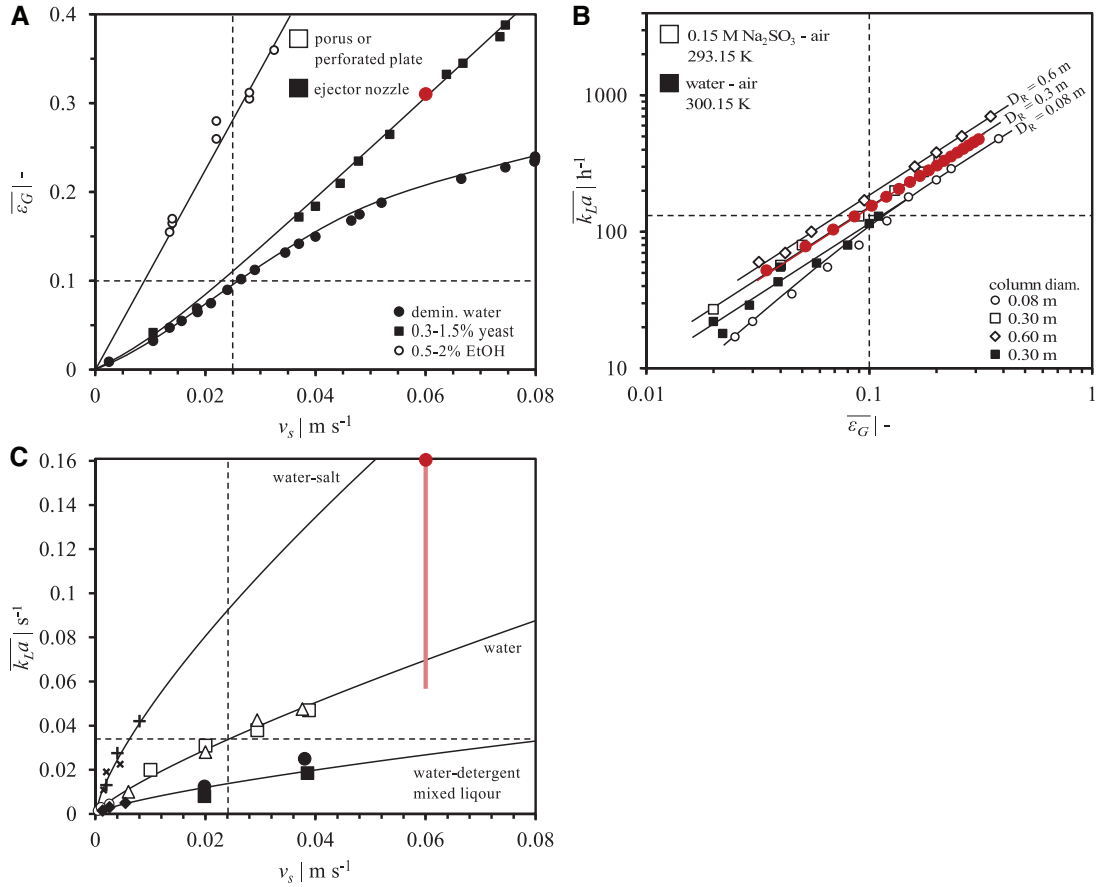

FIGURE 2 Comparing model predictions with experimental observations. In (A), the gas hold-up $\bar{\varepsilon}_G$ as a function of superficial gas velocity v_S for demineralized water, yeast solution, and ethanol solution is shown [27]. The average mass transfer rate $\overline{k_La}$ as a function of $\bar{\varepsilon}_G$ for different column diameters is depicted in (B) [28]. In (C), the $\overline{k_La}$ is shown as a function of superficial gas velocity v_S for water–salt solution, pure water, and water detergent mix [26]

with D_{CO} as the diffusion coefficient of CO in water [24, p. 127] and d_B as the bubble diameter. According to Tomiyama et al. [25], the steady-state uprising bubble velocity v_T can be estimated as

$$v_T = \sqrt{2}\left(\frac{\sigma g\left(\rho_L - \rho_G\right)}{\rho_L^2}\right)^{0.25} \tag{10}$$

for $2 \times 10^{-3} \leq d_B \leq 10 \times 10^{-3}$ m and Eötvös number $Eo = (\rho_L - \rho_G)\, g d_B/\sigma \leq 16$. With the measured surface tension of the cultivation medium $\sigma = 0.0724 \pm 0.0063$ N m (identified via bubble pressure tensiometer), the medium density $\rho_L = 1000$ kg m^{-3} and the air density $\rho_G = 1.2$ kg m^{-3} $v_T = 0.23$ m s^{-1} is calculated, which is pretty similar to the distilled water value $v_T = 0.25$ m s^{-1} [26]. The volume specific gas/liquid mass transfer area a was estimated assuming spherical bubbles:

$$a = \frac{6\varepsilon_G}{d_G} \tag{11}$$

For evaluating bubble diameters $\leq 10 \times 10^{-3}$ m, the following equation was applied:

$$\varepsilon_G = \frac{v_S}{v_T} \tag{12}$$

with $v_T = 0.23$ m s^{-1} [26]. Furthermore, the impact of media components such as organic acids, salts, and alcohols on ε_G and v_S were considered using the experimental findings of Schügerl et al. [27] as reference. By analogy, experimental observations of Heijnen and van't Ried [26] outlining the correlation between k_La and v_S regarding media compositions were used. Figure 2 provides an overview of the experimental measurements.

To challenge the plausibility of experimental findings, the model case of 0.06 vvm (i.e., superficial gas velocity $v_S = 0.025$ m s^{-1} in a 0.6 m bubble column) can be studied in Figure 2. For demineralized water, $\varepsilon_G = 0.1$ is indicated (Figure 2A, dashed line), which leads to k_La of about 130 h^{-1} (Figure 2C, dashed line). This is in agreement with the findings of Akita and Yoshida [28]. Accordingly, Figure 2 shows

the framework for further simulations. To be precise, the ethanol plot in Figure 2A is chosen as *C. ljungdahlii* also produce alcohols such as ethanol and 2,3-butanediol. Although the settings of v_T, D_{CO}, ρ_L, ρ_G, and σ could be fairly assumed as constant, ε_G, d_B, k_L, and k_La are intertwined according to Equations (9)–(12). Each simulation allowed the independent setting of two parameters, while the remaining two were calculated. The simulation scenarios A–E were performed using the following setting as reference (dashed black line): $y_{CO} = 0.55$, 0.06 vvm, $\bar{\varepsilon}_G = 0.1$ ($\varepsilon_{G,0} = 0.06$), and $\overline{k_La} = 130\ h^{-1}$ ($k_La = 90\ h^{-1}$ with $d_{B,0} = 5 \times 10^{-3}$ m and $k_L = 3.4 \times 10^{-3}\ m\ s^{-1}$).

1. Variation in CO gas fraction with $0 \leq y_{CO} \leq 0.9$.
2. Different gassing rates with $0.004 \leq v_S \leq 0.063$ m s^{-1} ($15 \leq \dot{V}_G \leq 225\ m^3\ s^{-1}$, 0.01–0.15 vvm).
3. Variations of k_La (ε_G = const.) with initial settings of 40–180 h^{-1} resulting in mean steady state values of $\overline{k_La}$ ranging from 60 to 250 h^{-1}.
4. Variation of initial gas hold-up $0.02 \leq \varepsilon_{G,0} \leq 0.19$ with fixed k_La resulting in $0.03 \leq \bar{\varepsilon}_G \leq 0.31$ (and variable d_B, see Figure S3 for explanation).
5. Same variation as in *D* but considering variable k_La yielding equal $\bar{\varepsilon}_G$ as in *D* and constant d_B (see Figure S3 for explanation).
6. Final parameter study with new reference set-up according to findings in *A* to *E*: $y_{CO} = 0.55$, 0.15 vvm and $\bar{\varepsilon}_G = 0.31$ ($\varepsilon_{G,0} = 0.19$). Initial k_La settings ranged from 100 to 425 h^{-1} finally reaching mean steady state $\overline{k_La}$ between 140 and 580 h^{-1}.

Figure 4 illustrates the observed sensitivities of the simulation scenarios A–E focusing on the readouts Y_{PX}(SS), C_{fix}(SS), $\bar{\varepsilon}_G$, $\bar{d}_B$, $\overline{k_La}$, and n_G. Values are normalized with respect to the maximum (1) and the minimum (−1) with the baseline (0) indicating the reference. Figure 3 provides an overview of the underlying data that were used for the sensitivity analysis in Figure 4.

The key observations are as follows:

(i) The physical parameters $\bar{\varepsilon}_G$, $\bar{d}_B$, $\overline{k_La}$, and n_G are neither dependent on the CO fraction y_{CO} nor on the gassing rate vvm (A,B). Rising CO fractions cause increasing CO fixation C_{fix}(SS), whereas reduction of y_{CO} leads to poor C_{fix}(SS) and production biomass yields Y_{PX}(SS). Interestingly, lowering gassing rates do not cause as severe reduction of Y_{PX}(SS).

(ii) Increasing k_La keeping $\bar{\varepsilon}_G$ constant leads to increasing bubble diameters and bubble numbers as indicated in *C*. As expected, C_{fix}(SS) and Y_{PX}(SS) improve with rising k_La and show lowered values for minimum settings.

(iii) Varying $\bar{\varepsilon}_G$ keeping k_La constant is responded by strong variations of bubble sizes and somewhat minor changes of bubble numbers. Impacts on the biological performance criteria are less pronounced.

(iv) Varying $\bar{\varepsilon}_G$ and liberating k_La caused the strongest amplitudes of the biological and the physical criteria except for the mean bubble diameter.

3.3 | Spatial and temporal results of 1-D approach

Simulation results of the 1-D approach applying the new reference setup are depicted in Figure 5. The time courses of biomass, acetate, ethanol, 2,3-butanediol, outlet gas (CO and CO_2), and mean dissolved CO and CO_2 clearly indicate steady-state process conditions after approximately 800 h. Notably, CO is completely consumed, whereas CO_2 is produced. The products acetate, ethanol, and 2,3-butanediol are constantly formed mirroring the experimental observations of *C. ljungdahlli* formulated in the stoichiometric model. During the first 2 h, the gas accumulates in the medium, since initial estimations of dissolved gas concentrations had not yet considered CO consumption and CO_2 formation with growing biomass.

The spatial analysis (B) reveals changing gas compositions over the column height. Dissolved CO levels are the highest at the bottom of the column, the only zone where growth inhibition (dissolved CO > 0.1 mmol L^{-1}) occurred according to Mohammadi et al. [22]. At about 11 m height, the carbon uptake rate severely dropped due to limiting CO levels ($c_{L,CO} \leq 0.014$ mmol L^{-1}). The model-based threshold value of $q_c = -14$ mmol $g_{CDW}^{-1}\ h^{-1}$ was fallen below. Consequently, by-product and biomass formation slow down. Notably, all by-product and biomass rates were spatially distributed that outlines their strict dependence on gas hold-up and mass transfer. Nevertheless, integral rates corresponded to the steady-state scenario of the entire bubble column.

3.4 | Comparison of 1-D with CFD results

Following the key motivation of this study to compare coarse grained 1-D modeling (F) with CFD, Table 1 provides an overview of the main results. As clearly depicted, almost all criteria reveal severe differences between 1-D (F) and CFD. By trend, the gas transfer simulated via 1-D (F) is much higher than via CFD. This is reflected by larger values of gas hold-up, mean bubble surface, k_L, and smaller mean bubble diameter. As a consequence, the mean k_La of 1-D (F) outnumbers the CFD values by factor 14 approximately. Noteworthy, mean dissolved CO values are predicted to be higher via 1-D (F) than via CFD. The 1-D model with set-up *F* overestimates the biological efficiency and predicts 40% more product biomass yield than CFD.

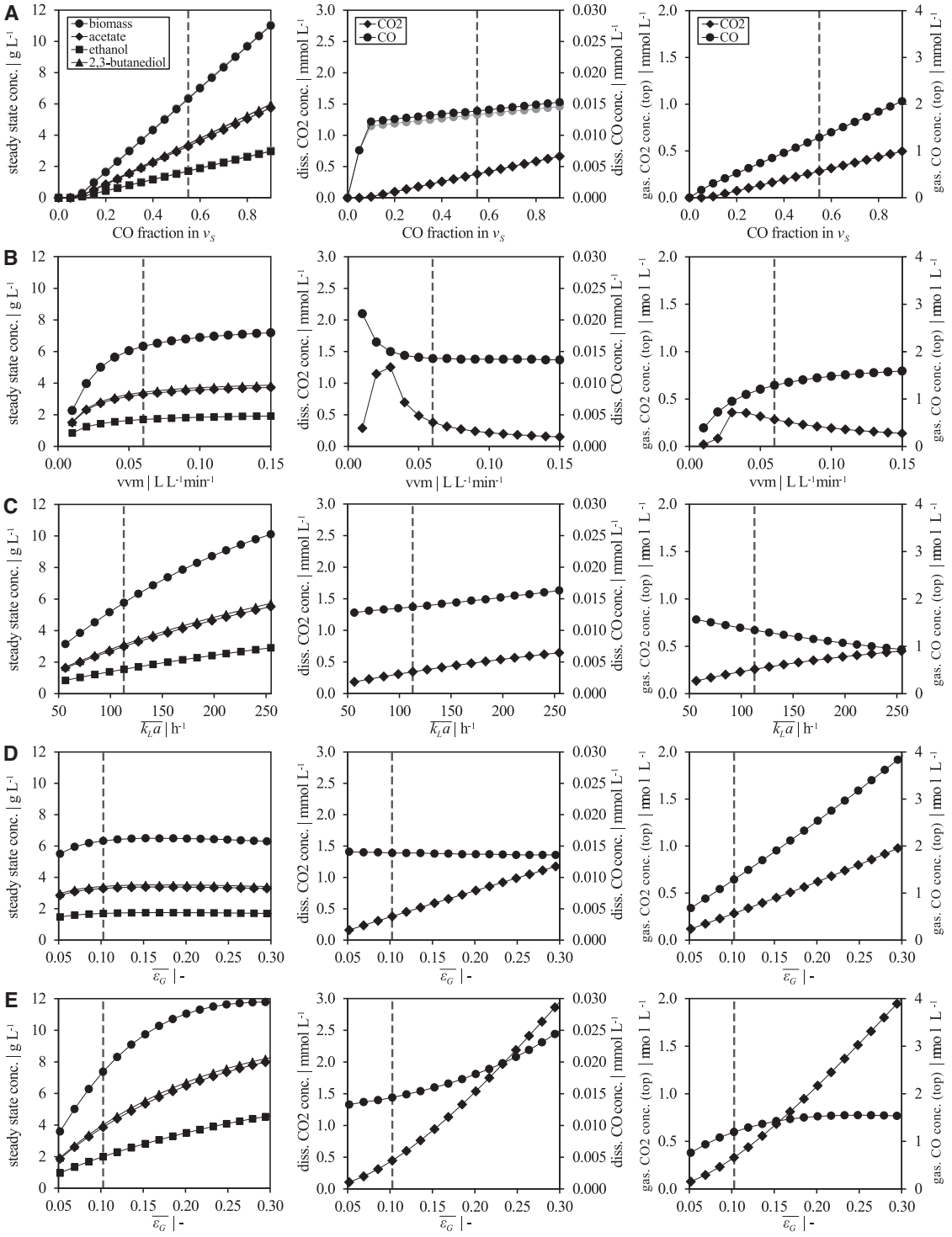

FIGURE 3 Steady-state results of parameter study. Variation of (A) gas composition, (B) gassing rate, (C) initial k_La value, (D) initial gas hold-up $\varepsilon_{G,0}$ with constant k_La value, and (E) initial gas hold-up $\varepsilon_{G,0}$ with variable k_La value. The reference set-up is indicated with a black dashed line. Gray points in (A) are simulation results without consideration of diffusion

In CA (F), the bubble diameter is way off too small in particular in the down part of the column. For this reason, a second run of the 1-D model (G) was conducted replacing the value by the Sauter mean diameter derived from CFD simulations. Results are indicated in Table 1 as 1-D (G) and in Figure 6 as red dashed line. This adaptation of the 1-D approach was further adjusted by approximating the initial gas hold-up and mass transfer rate according to the findings in the CFD approach.

Figure 6 illustrates the differences of 1-D (F), 1-D (G), 1-D*, and CFD simulation as a function of the column height. The trend of divergence depicted in Table 1 is clearly visible

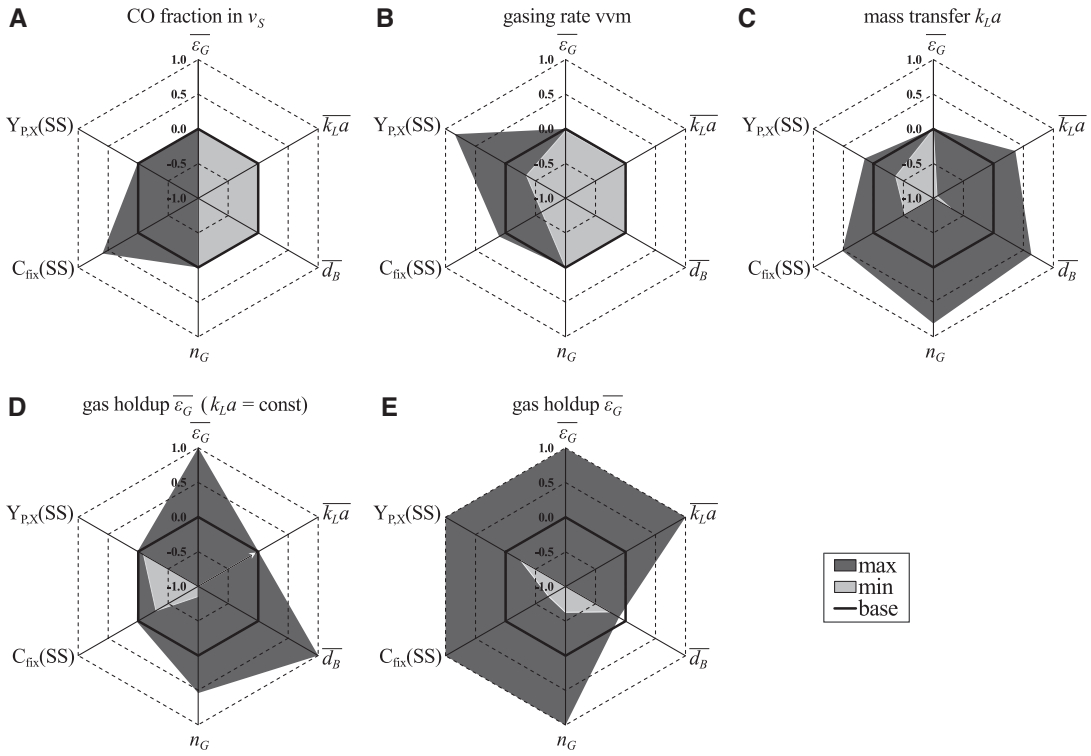

FIGURE 4 Parameter sensitivity analysis for conceptual design. The following scenarios are studied: (A) variation of gas composition (excluding wash-out results), (B) gassing rate, (C) initial k_La value, (D) initial gas hold-up $\varepsilon_{G,0}$ with constant k_La, and (E) initial gas hold-up $\varepsilon_{G,0}$ with variable k_La. Variables with a bar indicate the mean steady-state value. Additionally, the steady-state production biomass yields $Y_{P,X}$(SS), total steady-state carbon fixation C_{fix}(SS) and bubble number density n_G are depicted. All values are normalized to the maximum (1) as well as minimum (−1) value to allow comparability. The black solid line indicates the first parameter set thereby defining the baseline (0) of each radar graph. Areas of light gray (as well as small arrow in (D)) contour the set of minimum values, and dark gray areas encode maximum values

in the height-specific predictions using 1-D and CFD. Only within a small zone close to the bottom of the column 1-D and CFD, calculated gas hold-ups are equal. For all other cases, the above-mentioned criteria differ severely following the same trend as indicated in Table 1 (1-D (F) and CFD). Furthermore, Figure 6 also indicates the heterogeneity of the said values at each column height. In particular, CFD predicted bubble size distributions are very heterogeneous at each height, which also induces variations of gas hold-up. Additionally, using the gas hold-up and mass transfer value of CFD simulations improved the prediction quality of the 1-D model by 32% and 70% for bubble surface and volumetric mass transfer coefficient, respectively (see Table 1, 1-D (G) and 1-D*). The finding is in agreement with the observations of Bauer and Eigenberger [29] who suggested an iterative optimization strategy to optimize prediction quality of a so-called "zone" model. Notably, the statement holds equally true when additional biological readouts are considered: Acceptable 1-D model predictions can be achieved when Sauter diameter, gas hold-up, and mass transfer are derived from CFD simulations.

Figure 7 complements the comparison of the initial simulation results of 1-D (F) and (G) with CFD. The difference in percentage of the most diverging parameters, namely dissolved CO concentration, gas hold-up, and bubble diameter, is illustrated. By trend, CO levels are heavily overestimated almost everywhere using 1-D (F). Gas hold-ups of 1-D (F) and CFD are similar in the lower part of the column but are overestimated in the upper part. Figure 7 also provides detailed insights in the heterogeneities at each column height. Coloring indicates that severe discrepancies may even occur on the same height. The bottom and the upper part are particularly prone to heterogeneous conditions with respect to gas hold-up and bubble sizes.

4 | DISCUSSION

Intrinsically, 1-D modeling is a coarse-grained approach lumping local heterogeneities, thereby reducing the modeling complexity to a minimum. On contrast, CFD aims to unravel spatial particularities exploiting the local resolution. The latter is restricted by the maximum mesh size as well as the general model approach (e.g., multiphase) and therefore the resulting computational effort. For instance, resolving mixing and mass transfer of a 200-L stirred tank reactor with 500 k mesh yields a mean resolution of 0.5 mL and

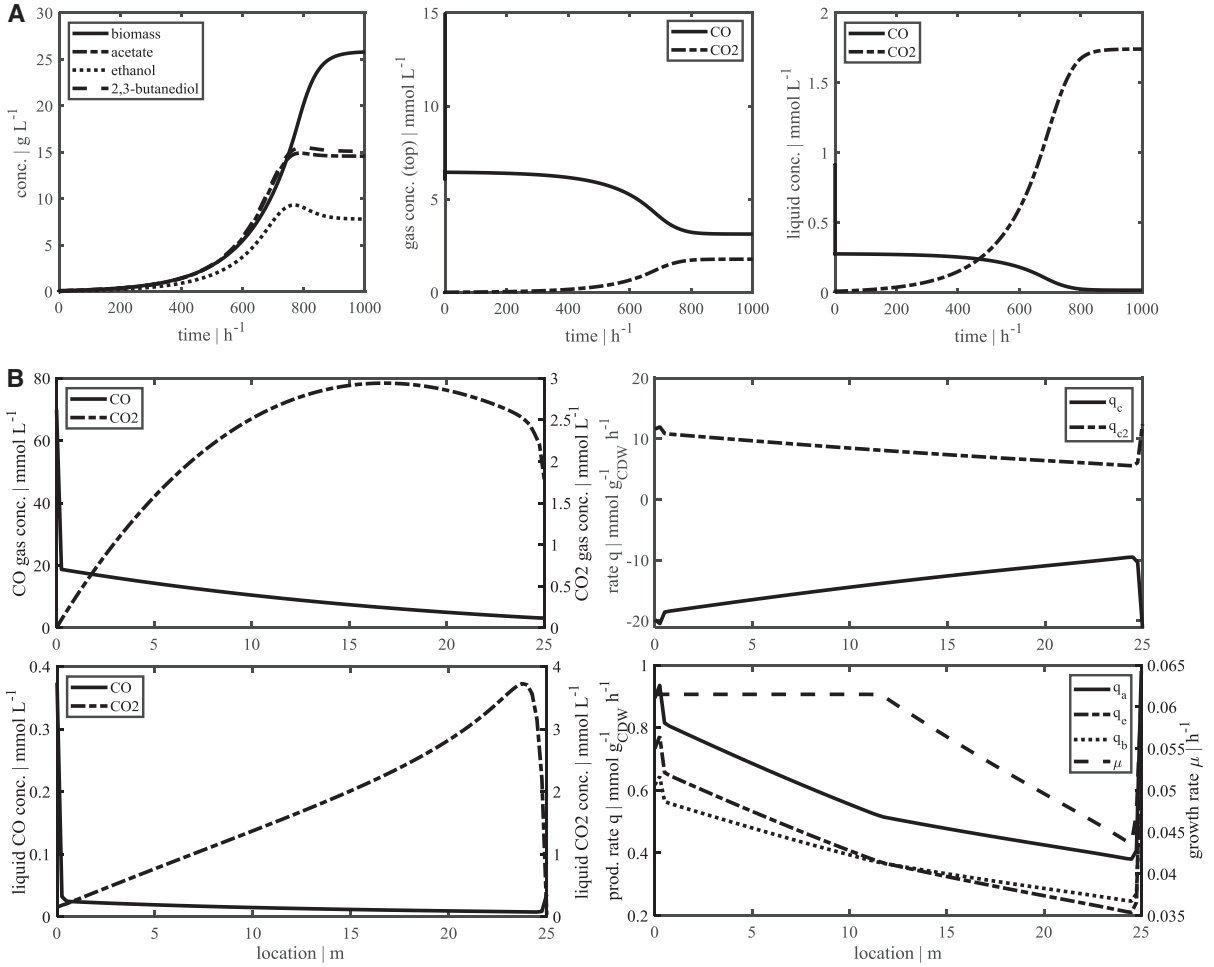

FIGURE 5 Temporal and spatial results for final parameter set-up. In (A), the average concentrations are pictured over time until the process reaches a steady state. (B) Spatially resolved steady-state results of the liquid and gaseous concentrations are shown on the left side. The right side illustrates the related consumption and production rates (acetate q_a, ethanol q_e, and 2,3-butanediol q_b and the growth rate μ)

TABLE 1 Average results of both simulation approaches in comparison

Average	Variable	1-D (F)	CFD	1-D (G)	1-D*	Units
CO concentration	$\bar{c}_{L,CO}$	0.018	0.002	0.016	0.0015	mmol L^{-1}
Gas hold-up	$\bar{\varepsilon}_G$	0.31	0.34/0.21[a]	0.31	0.21	–
Diameter	$\bar{d}_B$	4.4	20.9[b]	20.9	20.9	Mm
Bubble surface	$\bar{a}$	408.3	61.8	86.9	59.1	m^{-1}
Mass transfer rate	$\bar{k}_L$	3.93×10^{-4}	1.75×10^{-4}	3.93×10^{-4}	1.75×10^{-4}	m s^{-1}
Mass transfer	$\overline{k_L a}$	577	39	123	37	h^{-1}
Product-biomass yield	$\bar{Y}_{P,X}$	1.5	0.9	1.3	1.4	–

[a] Second value with breakage, coalescence, bubble expansion, and mass transfer.
[b] Sauter mean for CFD.
Both approaches, 1-D (1-D(F), (G) and *) and computational fluid dynamics (CFD) simulation used the same initial conditions with superficial gas velocity of 0.0625 m s-1 and initial bubble diameter of 4 mm. 1-D (G) used the Sauter mean diameter of the CFD simulation as mean bubble diameter. In the final simulation 1-D*, besides the Sauter diameter, the gas hold-up and mass transfer rate were adjusted accordingly. The product-biomass yield was calculated spatially with the correlation described in Siebler et al. [11].

requires about 2–3 days computing using state-of-the-art personal computers (here: calculation on 16 cores with double precision). However, demanding the same resolution for a 125 m^3 bioreactor calls for high-performance computing with supercomputers. As a consequence, evaluating tests probing different design sets for large-scale application need be performed in a less computationally challenging framework. Still, the same set of essential design parameters should be evaluated but computational speed allows for the identification of a preliminary design optimum that should

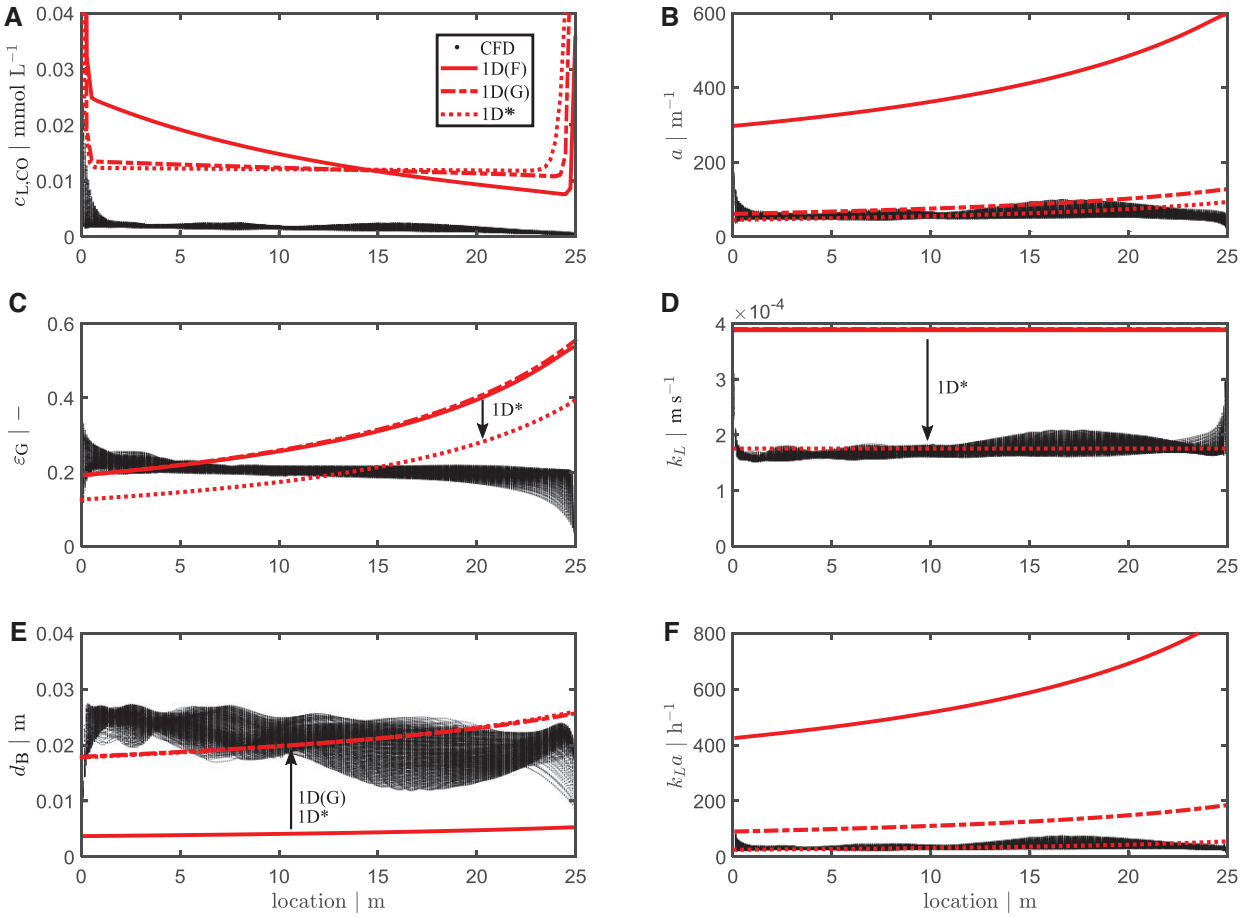

FIGURE 6 Profiles over reactor height in comparison. Each graph depicts profiles of CFD (dots) and 1-D (red lines) simulation. In case of CFD, each dot represents values of individual numerical cells, thereby visualizing the varying conditions at each column height. (A)–(F) Dissolved CO concentration $c_{L,CO}$, bubble area a, gas hold-up ε_G, mass transfer rate k_L, bubble diameter d_B, and volumetric mass transfer k_La are compared

be further investigated by CFD approaches. It is exactly this scenario that is exemplified in this study.

4.1 | Parameter space analysis

As indicated in Figs. 3 and 4, increasing CO fraction finally improves the biomass and the (by-)product formation indicated by the readouts C_{fix} and Y_{PX}. This observation reflects predominately low CO levels in the column which do not (yet) cause growth inhibition. Accordingly, any measure to improve CO levels is responded by rising C_{fix} and Y_{PX}. Noteworthy, the physical parameters $\bar{\varepsilon}_G$, $\bar{d}_B$, $\overline{k_La}$, and n_G are not affected by CO fractions, which allows their independent fine-tuning.

In agreement, variations of the gassing rate vvm support the necessity to install proper CO supply. Additionally, the important minimum threshold value of about 0.06 vvm is outlined (see Figure 4). Below, the biological readouts C_{fix} and Y_{PX} increase with strong positive correlation on vvm raise, whereas higher vvm settings improve biological performance only marginally. Accordingly, any gassing rate limitation beyond 0.06 vvm can be ruled out that renders this value an important design parameter. Noteworthy, low vvm settings may even cause maximum dissolved CO_2 levels, which reflect the counteracting mechanisms of gassing input, hold-up, and stripping.

The improvement of k_La values (variation C) is always beneficial for the biological readouts. Again, the finding mirrors the fact that most CO levels are far below inhibiting thresholds, which highlights the necessity to improve CO mass transfer.

One possibility to improve mass transfer is to increase gas hold-up. Equations (9)–(13) show that the set of related physical parameters is intertwined, linking changes of gas hold-up ε_G to changes of a, k_L, d_B, and k_La. For the sake of simplicity, large-scale simulations may exclude putative impacts of gas hold-up ε_G [14, 21]. However, this study aims to light related impacts by investigating two possible simulation regimes (see Figure S3): variation D keeps k_La constant; variation E allows flexible k_La (setting k_L and d_B constant with characteristic values, see Section 3.2).

The increase of ε_G (variation D) results in minor changes of the biological readouts (see Figure 4D). This reflects the fact that gas hold-up rise is responded by k_L reduction, which in turn reduces CO availability. However, the regime

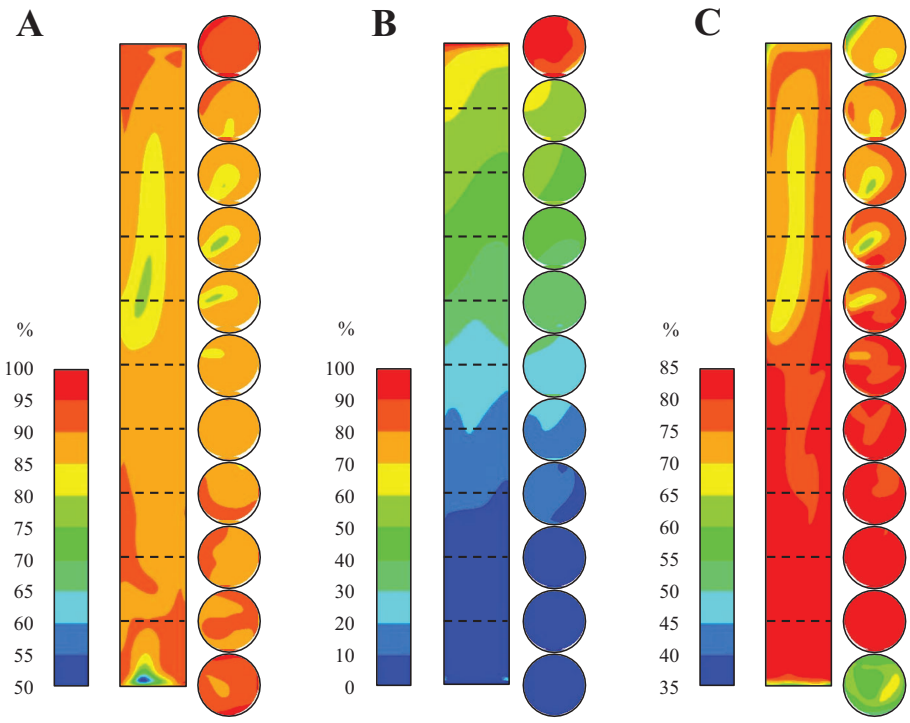

FIGURE 7 Differences between 1-D and CFD simulation over reactor height. Concentration $c_{L,CO}$ (A), gas hold-up ε_G (B), and mean diameter d_B (C) deviation profiles are demonstrated in percentage over the reactor height. Additionally, horizontal section planes (dashed lines, top and bottom) are graphically shown on the right side for each deviation profile. In (A), $100\% - c_{L,CO}^{CFD}(z)/c_{L,CO}^{1D}(z) \cdot 100\%$ is shown, which translates high similarity into low values. By analogy, graphic (B) is set. In (C), the criterion $100\% - d_B^{1D}(z)/d_B^{CFD}(z) \cdot 100\%$ was applied to avoid negative values. Still, high percentages encode large deviations

of variable $k_L a$ allows to transfer ε_G raise proportionally to rising a, which improves $k_L a$ and leads to alleviated process performance (see Figure 3E). Both cases illustrate that gas hold-up impacts have to be considered properly to get valid design values for further analysis.

Based on this evaluation, the setting of the reference process as the new optimal setting F was chosen as follows: The CO fraction was not adjusted since converter gas of metallurgical production processes rather not exceeds this value [30]. However, a moderate gassing rate of 0.15 vvm was chosen that responds to the gas hold up of $\varepsilon_G = 0.31$ ($\varepsilon_{G,0} = 0.19$). According to Bailey and Ollis [31, p. 611], this is the critical threshold value of starting heterogeneous bubbly flow in air–water systems. Finally, moderate to high mean steady-state $k_L a$ values range (140–580 h^{-1}) was rerun. The setting yielded the final simulation results in Figure 5.

4.2 | 1-D versus CFD

Figures 6 and 7 depict the discrepancy between 1-D and CFD modeling. Not only spatial differences are shown (Figure 7) but also discrepancies in fundamental trends (Figure 6). The first may have been expected as they reflect the missing granularity of 1-D modeling. However, the second clearly pinpoint to the lacking mechanistic details of modeling bubble size distributions with the 1-D (F) approach. Apparently, simply considering gas fractions and bubble numbers leads to severe overestimation of a values, which in turn reflect too small bubble diameters d_B. As a consequence, 1-D (F) overestimates $k_L a$, which creates too high CO levels and increases biological performance. Consequently, 1-D modeling should already consider proper approaches to simulate bubble sizes. Simply estimating bubble numbers creates biased simulation results. This trend was already indicated in the gas hold-up analysis and is clearly visible in Figure 6. Noteworthy, the consideration of the Sauter diameter of the CFD simulation improved the prediction quality of 1-D (G) with respect to physical and biological readouts. Additionally, using the gas hold-up and mass transfer value of CFD simulations enhanced simulation quality even further. Predictions of 1-D (G), 1-D*, and CFD converged but average rates and constants of mass transfer are still too high in 1-D (G). Nevertheless, the biological readouts approximated to approximately 40% deviation of the CFD value.

5 | CONCLUSIONS

Without doubt, CFD simulations inherently offer the most accurate prediction of physical and biological readouts, spatially resolved, in large-scale bioreactor fermentations. However, they also require detailed mechanistic understanding

and—equally challenging—proper computational power for dealing with industrial scale multiphase, mass transfer, mixing, and reaction problems. Conceptual design approaches need to search through parameter spaces of putative operational windows. Although CFD simulations would be ideal to fulfill the task, limited computational power constraints calculations on the use of 1-D models. Users must be aware that physical readouts are most likely overestimating bioreactor performance because impacts of bubbles are reflected poorly. Nevertheless, the use of properly estimated Sauter mean diameters from CFD helps to improve model predictions, in particular for highly relevant biological readouts such as product-biomass yields.

NOMENCLATURE

a	[m^{-1}]	Interfacial area concentration
A	[m^2]	Cross-sectional area
c_k	[g L^{-1}]	Product concentration
c_m	[mmol L^{-1}]	Gas concentration
C_{fix}(SS)	[-]	Total steady state carbon fixation
D	[h^{-1}]	Dilution rate
d_{32}	[m]	Sauter mean bubble diameter
d_B	[m]	Bubble diameter
D_{CO}	[m^2 s^{-1}]	Diffusion coefficient
D_L	[m^2 s^{-1}]	Liquid phase dispersion coefficient
D_R	[m]	Reactor diameter
$\mathbf{g}$	[m s^{-2}]	Gravitational acceleration
H_L	[m]	Liquid height
H_m^{cp}	[mol L^{-1} atm^{-1}]	Henry coefficient
k_L	[m s^{-1}]	Mass transfer coefficient
M	[g mol]	Molecular weight
n	[-]	Numerical volumes
N	[-]	Number of sections
N_B	[-]	Number of bubbles
n_G	[m^{-3}]	Number density
n_m	[mol]	Number of moles of gas
P	[atm]	Pressure
q_k	[mmol g_{CDW}^{-1} h^{-1}]	Production rates
$\dot{Q}_L$	[m^3 h^{-1}]	Media flow
q_m	[mmol g_{CDW}^{-1} h^{-1}]	Gas consumption rates
$\dot{Q}_R$	[m^3 h^{-1}]	Back flow
R	[$kg \cdot m^2 \cdot s^{-2} \cdot K^{-1} \cdot mol^{-1}$]	Universal gas constant
R_B	[m]	Bubble radius
t	[s]	Time
T	[K]	Temperature
v	[m s^{-1}]	Velocity
V	[m^3]	Volume
y_m	[-]	Gas fraction
Y_{PX}(SS)	[-]	Steady-state production biomass yields
z	[m]	Direction and unit of length
Δz	[m]	Section height
Greek symbols		
α	[-]	Combined back and media flow
ε	[-]	Volume fraction
μ	[h^{-1}]	Growth rate
ρ	[kg m^{-3}]	Density
ρ^*	[mol m^{-3}]	Total molar density
σ	[N m]	Surface tension
Indices		
*		Equilibrium concentration
0		Initial value
A		Acetate
B		2,3-Butanediol
B		Bubble
C		Indices for CO uptake rate
E		Ethanol
G		Gaseous
i		Section counter for 1-D approach
k		Product $k \in$ [acetate, ethanol, $2,3-$butanediol]
L		Liquid
m		Gas composition $m \in [CO, CO_2, H_2]$
R		Reactor
s		Indices superficial gas velocity
bubbles		Mass transfer area between the liquid and gaseous phase
slip		Slip velocity
T		Indices for terminal velocity
X		Biomass

ACKNOWLEDGMENTS

The authors would to thank the research group of Chen et al. [14, 20, 21] for their previous work on this subject. This work was supported by the Federal Ministry of Education and Research (BMBF; FKZ031A468B).

AUTHOR CONTRIBUTIONS

R.T. and A.L. proposed this study. Simulation and evaluation were conducted by Flora Siebler. The manuscript was written by F.S. and R.T.

CONFLICT OF INTEREST

The authors have declared no conflict of interest.

REFERENCES

1. Liguori, R., Faraco, V., Biological processes for advancing lignocellulosic waste biorefinery by advocating circular economy. *Bioresour. Technol.* 2016, *215*, 13–20.
2. Straathof, A.J.J., Wahl, S.A., Benjamin, K.R., Takors, R., et al., Grand research challenges for sustainable industrial biotechnology. *Trends Biotechnol*. 2019, *37*, 1042–1050.
3. Philp, J., The bioeconomy, the challenge of the century for policy makers. *N. Biotechnol.* 2018, *25*, 11–19.
4. Diender, M., Stams, A.J.M., Sousa, D.Z., Pathways and bioenergetics of anaerobic carbon monoxide fermentation. *Front. Microbiol.* 2015, *6*, 1–18.
5. Latif, H., Zeidan, A.A., Nielsen, A.T., Zengler, K., Trash to treasure: production of biofuels and commodity chemicals via syngas fermenting microorganisms. *Curr. Opin. Biotchnol.* 2014, *27*, 79–87.
6. Takors, R., Kopf, M., Mampel, J., Blümke, W., et al., Using gas mixtures of CO, CO_2 and H_2 as microbial substrates: the do's and don'ts of successful technology transfer from laboratory to production scale. *Microb. Biotechnol.* 2018, *11*, 606–625.
7. Bengelsdorf, F.R., Dürre, P., Gas fermentation for commodity chemicals and fuels. *Microb. Biotechnol.* 2017, *10*, 1167–1170.
8. Dürre, P., Butanol formation from gaseous substrates. *FEMS Microbiol. Lett.* 2016, *363*, fnw040.
9. Haringa, C., Tang, W., Deshmukh, A.T., Xia, J., et al., Euler-Lagrange computational fluid dynamics for (bio)reactor scale-down: an analysis of organism life-lines. *Eng. Life Sci.* 2016, 16, 652–663.
10. Kuschel, M., Siebler, F., Takors, R., Lagrangian trajectories to predict the formation of population heterogeneity in large-scale bioreactors. *Bioengineering* 2017, *4*, 1–13.
11. Siebler, F., Lapin, A., Hermann, M., Takors, R., The impact of CO gradients on *C. ljungdahlii* in a 125 m^3 bubble column: mass transfer, circulation time and lifeline analysis. *Chem. Eng. Sci.* 2019, 207, 410–423.
12. Haringa, C., Tang, W., Wang, G., Deshmukh, A.T., et al., Computational fluid dynamics simulation of an industrial *P. chrysogenum* fermentation with a coupled 9-pool metabolic model: towards rational scale-down and design optimization. *Chem. Eng. Sci.* 2018, *175*, 12–24.
13. Zieringer, J., Takors, R., In silico prediction of large-scale microbial production performance: constraints for getting proper data-driven models. *Comput. Struct. Biotechnol. J.* 2018, *16*, 246–256.
14. Chen, J., Gomez, J.A., Höffner, K., Phalak, P., et al., Spatiotemporal modeling of microbial metabolism. *BMC Syst. Biol.* 2016, *10*, 1–13.
15. Lapin, A., Lübbert, A., Numerical simulation of the dynamics of two-phase gas—liquid flows in bubble columns. *Chem. Eng. Sci.* 1994, *49*, 3661–3674.
16. Vrábel, P., van der Lans, R.G.J.M., van der Schot, F.N., Luyben, K.C.A.M., et al., CMA: integration of fluid dynamics and microbial kinetics in modelling of large-scale fermentations. *Chem. Eng. J.* 2001, *84*, 463–474.
17. Heins, A.-L., Lencastre Fernandes, R., Gernaey, K. V., Lantz, A.E., Experimental and in silico investigation of population heterogeneity in continuous *Sachharomyces cerevisiae* scale-down fermentation in a two-compartment setup. *J. Chem. Technol. Biotechnol.* 2015, *90*, 324–340.
18. Pigou, M., Morchain, J., Investigating the interactions between physical and biological heterogeneities in bioreactors using compartment, population balance and metabolic models. *Chem. Eng. Sci.* 2015, *126*, 267–282.
19. Delafosse, A., Collignon, M.-L., Calvo, S., Delvigne, F., et al., CFD-based compartment model for description of mixing in bioreactors. *Chem. Eng. Sci.* 2014, *106*, 76–85.
20. Chen, J., Gomez, J.A., Höffner, K., Barton, P.I., et al., Metabolic modeling of synthesis gas fermentation in bubble column reactors. *Biotechnol. Biofuels* 2015, *8*, 1–12.
21. Chen, J., Daniell, J., Griffin, D., Li, X., et al., Experimental testing of a spatiotemporal metabolic model for carbon monoxide fermentation with *Clostridium autoethanogenum*. *Biochem. Eng. J.* 2018, *129*, 64–73.
22. Mohammadi, M., Mohamed, A.R., Najafpour, G.D., Younesi, H., et al., Kinetic studies on fermentative production of biofuel from synthesis gas using *Clostridium ljungdahlii*. *Sci. World J.* 2014, *2014*, 1–8.
23. Higbie, R., The rate of absorption of a pure gas into a still liquid during short periods of exposure. *Trans. Am. Inst. Chem. Eng.* 1935, *35*, 365–389.
24. Cussler, E.L., *Diffusion: Mass Transfer in Fluid Systems*, 3rd ed., Cambridge University Press, Cambridge, UK 2009.
25. Tomiyama, A., Kataoka, I., Zun, I., Sakaguchi, T., Drag coefficients of single bubbles under normal and micro gravity conditions. *Japan Soc. Mech. Eng.* 1998, *41*, 472–479.
26. Heijnen, J.J., van't Riet, K., Mass transfer, mixing and heat transfer phenomena in low viscosity bubble column reactors. *Chem. Eng. J.* 1984, *28*, 21–42.
27. Schügerl, K., Lücke, J., Oels, U., Bubble column bioreactors: tower bioreactors without mechanical agitation. *Adv. Biochem. Eng.* 1977, 1–84.
28. Akita, K., Yoshida, F., Gas holdup and volumetric mass transfer coefficient in bubble columns. Effects of liquid properties. *Ind. Eng. Chem. Process Des. Dev.* 1973, *12*, 76–80.
29. Bauer, M., Eigenberger, G., A concept for multi-scale modeling of bubble columns and loop reactors. *Chem. Eng. Sci.* 1999, *54*, 5109–5117.
30. Clarke Energy ®. Furnace Gas for Power Production: Gases from Metallurgical Production Processes. Clarke Energy, Algeria 2018.
31. Bailey, J.E., Ollis, D.F., *Biochemical engineering fundamentals*, 2nd ed. Chemical Engineering Education, Mc Graw-Hill Inc., USA 1986.

SUPPORTING INFORMATION

Additional supporting information may be found online in the Supporting Information section at the end of the article.

How to cite this article: Siebler F, Lapin A, Takors R. Synergistically applying 1-D modeling and CFD for designing industrial scale bubble column syngas bioreactors. *Eng Life Sci*. 2020;20:239–251. https://doi.org/10.1002/elsc.201900132